

Chemical and structural analysis of the Large Magellanic Cloud using the fundamental mode RR Lyrae stars

Sukanta Deb^{*}, Harinder P. Singh

Department of Physics & Astrophysics, University of Delhi, Delhi 110007, India

Received on ; Accepted on

ABSTRACT

We present a careful and detailed light curve analysis of publicly available I -band data on fundamental mode RR Lyrae (RRab) stars of the Large Magellanic Cloud (LMC) obtained by the Optical Gravitational Lensing Experiment (OGLE) phase-III project. Using the Fourier parameters of 13,095 RRab stars, metallicities and absolute magnitudes of individual stars are obtained. The representation of stars on the $P - \phi_{31}^V$ plane shows the existence of three significant metallicity groups with mean metallicities as -1.20 ± 0.12 dex, -1.57 ± 0.10 dex and -1.89 ± 0.09 dex. The corresponding absolute magnitudes of these three groups are obtained as 0.70 ± 0.08 mag, 0.59 ± 0.06 mag and 0.49 ± 0.08 mag, respectively. Distribution of these three groups as a function of vertical $|z|$ distance indicates that the formation of the LMC disk predates the formation of the inner halo. Issue of the existence of a metallicity gradient as a function of galactocentric distances has also been addressed.

Approximating the structure of the LMC disk as a triaxial ellipsoid, the inclination angle (i) relative to the plane of the sky and the position angle of the line of nodes (θ_{lon}) were estimated as $24^\circ.20$ and $176^\circ.01$, respectively. The axes ratios and the eccentricity were also determined using the principal axes transformation method.

Key words: stars: variables: RR Lyrae-stars:fundamental parameters - stars: Population II - galaxies: statistics - galaxies:structure - galaxies:Magellanic Clouds

1 INTRODUCTION

The presence of old stellar populations like the pulsating RR Lyrae (RRL) stars, identified and characterized in large numbers in the LMC by recent automated surveys such as OGLE, serve as an invaluable tool to unlock the secret of the galaxy. The core helium burning pulsating RRL stars are excellent standard candles to estimate the Galactic and extragalactic distances and obey well defined luminosity-metallicity and period-luminosity-metallicity relations in optical and near infrared photometric bands (Butler 2003; Catelan et al. 2004; Sollima et al. 2006; Cáceres & Catelan 2008; Klein et al. 2011). In the V -band, the brightness of a RRL star is nearly standard with a slight metallicity dependence (Klein et al. 2011). They can be easily identified by their distinctive light curves. The presence of RRL stars in globular clusters facilitates the estimation of their ages and, hence, helps constrain the lower bound on the age of the Universe (Clementini 2010; de Grijs 2011; Majaess et al. 2012). The RRL stars are being used to determine the cosmological distance scale, the interstellar extinction along

the line of sight and to create a three dimensional map of different galaxies (Subramanian & Subramanian 2012; Haschke et al. 2012).

The LMC serves as an important target in the calibration of cosmic distance scale because of its proximity and low inclination angle. This galaxy hosts a statistically large sample of ‘standard candles’ which includes RRL, Cepheids and Red Clump giant stars. The accurate distance determination to the LMC plays a significant role in constraining the value of the Hubble constant H_0 (Schaefer 2008; de Grijs 2011; Riess et al. 2011). The distance measurement to the LMC has revolutionized our understanding of the distance scale of the Universe and supported the evidence for the expansion of the Universe (Challouf et al. 2012). The unique location of the LMC along with the abundance of various types of ‘standard candles’ allows us to compare and calibrate a large sample of distance indicators, which in turn can be utilized for more distant objects (de Grijs 2011).

Generally, the distances can be measured more accurately from the binary star light curve modelling using the combined photometric and spectroscopic data (Vilardell et al. 2010; Deb & Singh 2011; Challouf et al. 2012; Pietrzyski et al. 2013). Recently, using the surface-

^{*} E-mail: sukantodeb@gmail.com

brightness/color relation of the components of eight binary systems in the LMC, the angular sizes of the components were combined with their linear dimensions obtained from the light curve modeling to obtain the distance modulus of the LMC as $(m - M)_0 = 18.493 \pm 0.008(\text{statistical}) \pm 0.047(\text{systematic})$ mag (Pietrzyski et al. 2013). This corresponds to a distance of $49.97 \pm 0.19(\text{statistical}) \pm 1.11(\text{systematic})$ kpc, accurate to 2%. Most of the systems were located near the center of the LMC and situated along the line of nodes (Pietrzyski et al. 2013).

The LMC is a late type disk galaxy seen nearly face-on with enormous amount of gas, dust and inhabits sites for active star formation. There is a spectacular evidence of ongoing interactions with both the Milky Way and the Small Magellanic Cloud (Lin et al. 1995; Westerlund 1997; Subramanian & Subramanian 2010). The depth of the LMC is a few kpc along the line of sight. The geometry and orientation of the disk galaxy such as LMC has been the subject of numerous studies through the use of different tracers. The issue of the LMC geometry has major implications. Until the last decade, our understanding of the LMC was shallow due to the small number of tracers and availability of the data with limited spatial coverage (van der Marel & Cioni 2001; Weinberg & Nikolaev 2001; Subramanian 2003; Nikolaev et al. 2004; Subramanian & Subramanian 2009; Cioni 2009; Subramanian & Subramanian 2013). The LMC has been the best astrophysical laboratory for studies of various stellar populations, interstellar matter, star-formation processes and the galactic structure at large (Fukui & Kawamura 2010; Glatt et al. 2010).

The OGLE database has become a valuable resource for studying the properties of variable stars as it contains a pool of light curve data of a variety of variables present in our Galaxy as well as the nearby satellite galaxies, viz., the LMC and the SMC (Small Magellanic Cloud). The present paper attempts to use the wealth of RRL data of LMC from the OGLE-III catalog in order to unravel the various chemical and structural properties of this galaxy. A proper and systematic light curve analysis of the LMC RRab stars has been carried out in order to comprehend the metallicity and distance distribution of these tracers. These parameters along with the others have been utilized in deciphering the structure of the LMC. The independent analysis based on the RRab stars done in this paper will serve as a source to compare and correlate with the determinations of structural parameters of the LMC, such as inclination (i) and position angle of the line of nodes (θ_{lon}), derived from other studies using different tracers and methodologies.

In order to make the OGLE data more useful, we have cleaned the phased light curves using 2σ clipping. The clean phased light curves were then Fourier decomposed in order to determine the various parameters and their associated errors. This paper will, thus, serve as a supplementary and advanced version of the OGLE catalog of the LMC RRab stars, in which all the useful Fourier parameters are provided.

The Fourier parameters determined from the light curves of RRab stars are useful for distance determinations and metal abundance of the galaxy in which they are present. The past research has proved that the shape of a RRL light curve can be described in terms of the Fourier parameters that can be linked with the physical param-

eters such as mass (M), radius (R), and luminosity (L) of the star. They can also be linked to the other atmospheric parameters, such as metallicity ($[Fe/H]$), effective temperature (T_{eff}) and surface gravity ($\log g$) of the RRL stars (Jurcsik & Kovacs 1996; Kovacs & Jurcsik 1996; Jurcsik 1998; Kovacs & Kanbur 1998; Kovács & Walker 2001). Nevertheless, it has also been shown by Cacciari et al. (2005) that the intrinsic colors derived from Fourier coefficients show discrepancies with the observed ones, and hence the resulting temperatures and temperature-related parameters are unreliable.

The paper is organized as follows. In section 2, we describe the sample of RRab stars in the OGLE-III LMC database (Soszyński et al. 2009, hereafter, SZ09). The Fourier decomposition method as applied to the RRab light curves in the I -band and the sample selection criteria are described in section 3. Section 4 describes the determination of metallicities and absolute magnitudes of the RRab stars using the calibration relations between I and V -bands and then using the resulting V -band parameters in the empirical relations from the literature. Distance determination to individual RRab stars of the LMC using the intensity weighted mean magnitudes, the absolute magnitudes and the interstellar extinction has also been discussed. In section 5, we describe the determination of the structural parameters of the LMC by plane fitting procedure and principal axes transformation method using the moment of inertia tensor constructed from the projected three dimensional Cartesian coordinates of RRab stars. Dependence of the geometrical parameters on the choice of the LMC center is discussed. Comparison with other studies in the literature is provided. Section 6 discusses the issue of metallicity gradient in the LMC as a function of galactocentric distance (R_{GC}) using the metallicity values obtained from four different empirical relations available in the literature. Finally, in section 7, the summary and the conclusions of the present study are laid down.

2 THE DATA

We selected RRab stars from OGLE-III catalog that consists of 8-year archival data identified and characterized by the Fourier coefficients of the light curves (SZ09). The catalog contains 17,693 RRab stars having a mean period of $\langle P_{ab} \rangle = 0.576$ days. The OGLE field in the LMC covers nearly 40 deg^2 . Most of the observations were carried out using the Cousins I -band filter with exposure time of 180s having an average of 400 photometric observations. The catalog also contains V -band light curves of 17,337 stars having an average of 30 data points per light curve. The color ($\langle V \rangle - \langle I \rangle$)-magnitude ($\langle I \rangle$) diagram for 17,337 stars is shown in Fig. 1, where $\langle V \rangle$ and $\langle I \rangle$ are the intensity weighted mean magnitudes in the V and I -band, respectively and are obtained from the Fourier fitted light curves. Fig. 2 shows the plot of reddening free Wesenheit index (W_{VIc}) as a function of pulsation period (P) of the 17,337 RRab stars, where W_{VIc} is defined as $W_{VIc} = \langle I \rangle - 1.55(\langle V \rangle - \langle I \rangle)$ (Soszyński et al. 2003). Also overplotted on the data points is the fit from the empirical relation (Soszyński et al. 2003)

$$W_{VIc} = (-2.75 \pm 0.04) \log P + (17.217 \pm 0.008). \quad (1)$$

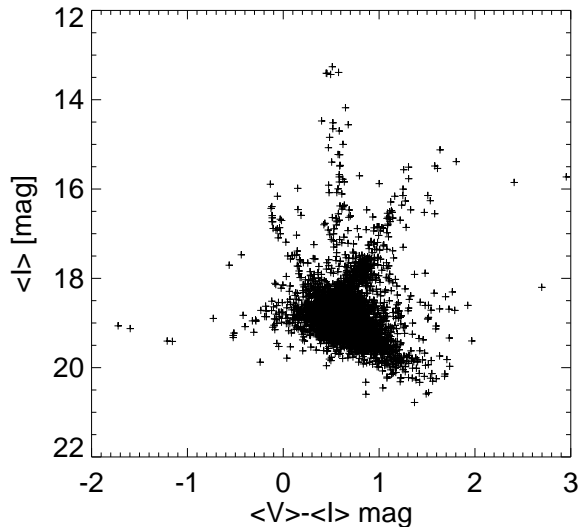


Figure 1. Color-magnitude diagram of the 17,337 RRab stars which have both I and V -band light curves available in the OGLE-III catalog.

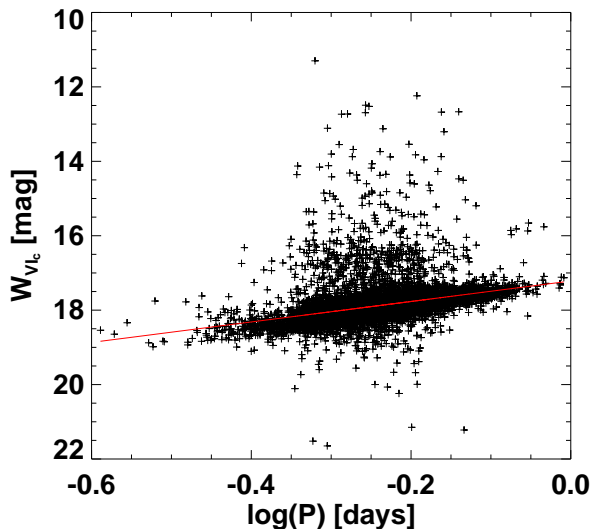


Figure 2. Wesenheit index (W_{VIc}) as a function of pulsation period (P) of the 17,337 LMC RRab stars which have both I and V -band light curves available in the OGLE-III catalog. Solid line represents the fit to the observed data points from the empirical relation of Soszynski et al. (2003) as given by Eqn. 1.

The empirical slope of the function is consistent with that predicted by models (Di Criscienzo et al. 2004).

For the analysis of light curves of RRab stars, we have selected the I -band data as they contain relatively larger number of data points per light curve as compared to corresponding V -band light curves. The OGLE-III light curve data of the LMC central region are further supplemented by the OGLE II data collected between 1997 and 2000 using the same telescope set up. The catalog contains intensity I and V -band mean magnitudes, periods and their uncertainties in

days, epochs of maximum light, peak-to-peak I -band magnitudes and the Fourier parameters R_{21} , Φ_{21} , R_{31} and Φ_{31} derived from the I -band light curves.

3 FOURIER DECOMPOSITION METHOD AND SAMPLE SELECTION

The Fourier decomposition method described below was used to obtain various light curve parameters of the LMC RRab stars. The light curves were fitted with a Fourier cosine series of the form

$$m(t) = A_0 + \sum_{i=1}^N A_i \cos(i\omega(t - t_0) + \phi_i), \quad (2)$$

where $m(t)$ is the observed magnitude, A_0 is the mean magnitude, $\omega = 2\pi/P$ is the angular frequency, P is the period of the star in days and t is the time of observation. The epoch of maximum light t_0 is used to obtain a phased light curve which has maximum light at phase zero. A_i 's and ϕ_i 's are the i th order Fourier coefficients and N is the order of the fit. Eqn. 2 has $2N + 1$ unknown parameters. To solve for these parameters, we require at least the same number of data points. The light curves were phased using

$$\Phi = \frac{(t - t_0)}{P} - \text{Int} \left(\frac{(t - t_0)}{P} \right).$$

The pulsation periods (P) and the t_0 values are taken from the OGLE catalog. An automated code was developed using the MPFIT package in IDL to obtain various Fourier parameters on the right hand side of Eqn. 2 (Deb & Singh 2010). A seventh order Fourier fit was employed to model the RRab I -band light curves. The Fourier fitted I -band light curves of a sample of RRab stars are shown in Fig. 3. The phase differences, $\phi_{i1} = \phi_i - i\phi_1$ and amplitude ratios, $R_{i1} = (A_i/A_1)$, $i > 1$ were evaluated and standard errors were determined using the formulae of Deb & Singh (2010).

In order to have a clean sample of RRab stars for the present analysis, we have used the selection criteria based on OGLE-determined periods, the mean magnitude (A_0) and the peak-to-peak I -band amplitude (A_I) determined from the Fourier analysis of the cleaned phased light curves. We chose RRab stars with period $P \geq 0.4$ days, mean magnitude $A_0 \geq 17$ mag and amplitude $0.1 \leq A_I \leq 1.2$ mag. These selection criteria were applied in order to exclude the RRc stars and the high amplitude δ Scuti stars that may have been misclassified as RRab stars, thus ensuring a reliable sample of RRab stars for the present analysis. The application of these selection criteria reduces the number of RRab stars in the I -band light curves to 17,092. The period-amplitude diagram for the complete and the selected sample of 17,092 RRab stars is shown in Fig. 4. In order to select the ‘normal-looking’ RRab stars out of 17,092 stars, the application of the compatibility test of Jurcsik & Kovacs (1996) further reduces the number of stars to 13,095. These 13,095 stars were retained for the physical parameter estimation and determination of the structure of the LMC in the present study. The equatorial coordinates (α , δ) of the selected sample of 13,095 RRab stars are shown in Fig. 5. The centroid of the final sample is $(\alpha_0, \delta_0) = (80^\circ.35, -69^\circ.65)$ and is shown as a filled circle in the figure. The Fourier pa-

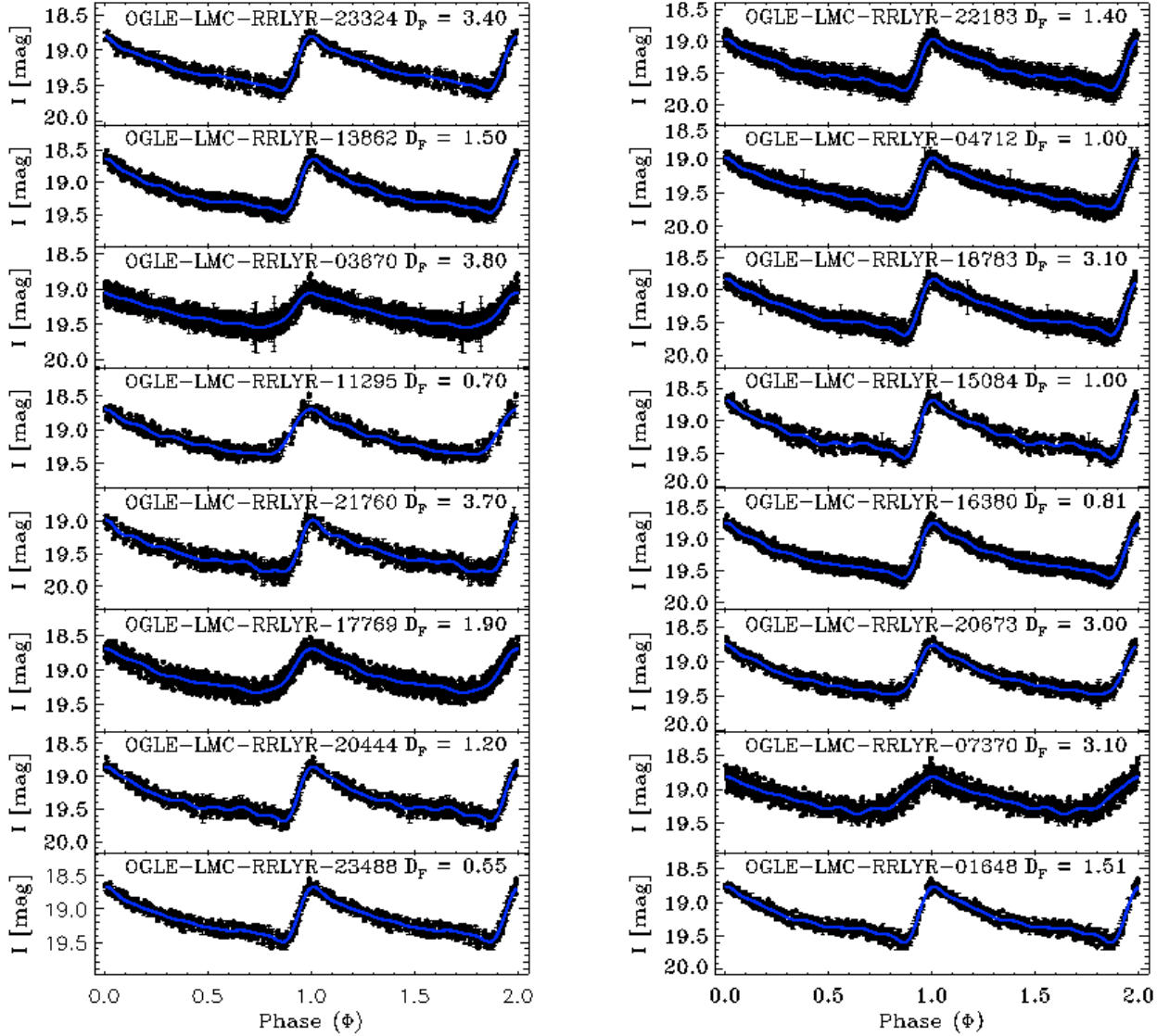


Figure 3. Fourier fitted R-Rab light curves in the I -band from the catalog. The quantity D_F represents the deviation parameter as defined by Jurcsik & Kovacs (1996) and is discussed in section 4.1.

rameters obtained from the Fourier decomposition method are listed in Tables 1 and 2, respectively.

In order to make a comparison of the parameters obtained in the present study with those given in the OGLE-III catalog, scatter plots of the Fourier amplitudes R_{21} , R_{31} and the phase parameters ϕ_{21} , ϕ_{31} are shown in Fig. 6. For the I -band data under consideration, the Fourier amplitude ratios R_{21} , R_{31} and R_{41} as a function of $\log(P)$ are shown in Fig. 7. The plot of the Fourier phase parameters ϕ_{21} , ϕ_{31} and ϕ_{41} as a function of $\log(P)$ is shown in Fig. 8. The dispersion in the ϕ_{i1} values ($i = 2, 3, 4$) goes on increasing as we go to higher orders. This is because the uncertainty in the determination of the Fourier phase parameters increases as one goes to higher orders. Fig. 8 illustrates that ϕ_{21} and ϕ_{31} increase with increasing period. On the contrary, there

is no clear trend for ϕ_{41} which is accounted for by their large uncertainties.

In Fig. 9, the estimated errors for R_{21} , R_{31} , and R_{41} are plotted. The distribution of the errors are similar for all the three Fourier amplitudes. On the other hand, from Fig. 10 we can see that the errors in ϕ_{41} are larger than those of ϕ_{21} and ϕ_{31} , whereas, in turn the errors in ϕ_{31} are larger than that of ϕ_{21} . This is expected as the amplitudes for the higher orders become smaller and smaller, it becomes increasingly difficult to derive their phases with high precision.

Table 1. A sample of the Fourier parameters of 13,095 OGLE RRab stars with increasing period used for the analysis obtained from the Fourier cosine decomposition of the I -band light curves as given by Eqn. 2. The full table is available as supplementary material in the online version of this paper.

OGLE ID	P[days]	A_0 σ_{A_0}	A_1 σ_{A_1}	A_2 σ_{A_2}	A_3 σ_{A_3}	A_4 σ_{A_4}	ϕ_1 σ_{ϕ_1}	ϕ_2 σ_{ϕ_2}	ϕ_3 σ_{ϕ_3}	ϕ_4 σ_{ϕ_4}
OGLE-LMC-RRLYR-23488	0.4003274	19.16019 0.00427	0.25560 0.00529	0.13633 0.00586	0.09880 0.00584	0.06321 0.00596	2.27497 0.02633	2.40845 0.04545	2.77793 0.06294	3.21414 0.09666
OGLE-LMC-RRLYR-20444	0.4005525	19.35242 0.00509	0.25310 0.00641	0.15458 0.00719	0.10378 0.00721	0.05028 0.00719	2.33045 0.03139	2.35537 0.04714	2.79613 0.06972	3.13930 0.14416
OGLE-LMC-RRLYR-17769	0.4009905	19.07511 0.00173	0.24234 0.00229	0.11507 0.00239	0.04785 0.00244	0.01949 0.00242	2.49946 0.01071	2.78721 0.02173	3.39620 0.05121	3.82907 0.12683
OGLE-LMC-RRLYR-21760	0.4011895	19.48245 0.00548	0.25007 0.00713	0.14082 0.00765	0.09722 0.00764	0.05027 0.00768	2.25690 0.03306	2.41177 0.05525	2.97533 0.08149	3.15050 0.15664
OGLE-LMC-RRLYR-11295	0.4017449	19.11341 0.00399	0.25864 0.00492	0.11954 0.00509	0.05925 0.00528	0.03505 0.00547	2.50487 0.02415	2.94624 0.05108	3.36518 0.09987	3.90536 0.16220
OGLE-LMC-RRLYR-03670	0.4017562	19.33933 0.00299	0.19194 0.00408	0.07938 0.00417	0.03781 0.00420	0.02109 0.00421	2.41474 0.02274	2.83343 0.05401	3.41382 0.11244	3.72526 0.20248
OGLE-LMC-RRLYR-13862	0.4018669	19.15250 0.00226	0.26409 0.00295	0.14338 0.00315	0.09822 0.00315	0.05805 0.00313	2.31965 0.01298	2.37446 0.02263	2.84023 0.03305	3.06405 0.05609
OGLE-LMC-RRLYR-23324	0.4019162	19.25332 0.00458	0.24472 0.00642	0.13560 0.00625	0.08229 0.00645	0.05855 0.00636	2.28630 0.02656	2.50185 0.04917	3.08952 0.07859	3.35738 0.11124
OGLE-LMC-RRLYR-01648	0.4020618	19.24330 0.00407	0.25264 0.00512	0.15037 0.00566	0.09507 0.00571	0.05554 0.00550	2.25824 0.02521	2.30472 0.03935	2.71777 0.06000	3.19910 0.10625
OGLE-LMC-RRLYR-07370	0.4025514	19.13236 0.00241	0.21665 0.00327	0.06850 0.00341	0.03027 0.00346	0.01456 0.00343	2.65053 0.01641	3.18102 0.04971	3.46347 0.11048	3.24620 0.23261

Table 2. A sample of the Fourier parameters of 13,095 OGLE RRab stars with increasing period used for the analysis obtained from the Fourier cosine decomposition of the I -band light curves as given by Eqn. 2. The full table is available as supplementary material in the online version of this paper.

OGLE ID	N_{obs}	χ^2_ν	σ_{fit}	A_I σ_{A_I}	R_{21} $\sigma_{R_{21}}$	R_{31} $\sigma_{R_{31}}$	R_{41} $\sigma_{R_{41}}$	ϕ_{21} $\sigma_{\phi_{21}}$	ϕ_{31} $\sigma_{\phi_{31}}$	ϕ_{41} $\sigma_{\phi_{41}}$
OGLE-LMC-RRLYR-23488	319	0.73841	0.05952	0.82006 0.10851	0.53339 0.02544	0.38655 0.02420	0.24731 0.02388	4.14170 0.05252	2.23621 0.08206	0.39746 0.12483
OGLE-LMC-RRLYR-20444	313	0.67103	0.06892	0.83119 0.12521	0.61074 0.03235	0.41004 0.03033	0.19865 0.02885	3.97765 0.05664	2.08796 0.09382	0.10067 0.17220
OGLE-LMC-RRLYR-17769	947	2.73231	0.08563	0.64168 0.09974	0.47482 0.01084	0.19746 0.01024	0.08044 0.01001	4.07149 0.02422	2.18101 0.05551	0.11443 0.13083
OGLE-LMC-RRLYR-21760	308	0.83825	0.08641	0.79528 0.03947	0.56310 0.03457	0.38876 0.03251	0.20104 0.03124	4.18116 0.06438	2.48782 0.10494	0.40610 0.18540
OGLE-LMC-RRLYR-11295	319	1.48647	0.07479	0.67497 0.04823	0.46218 0.02157	0.22907 0.02089	0.13552 0.02129	4.21969 0.05650	2.13376 0.11093	0.16907 0.17764
OGLE-LMC-RRLYR-03670	889	0.91742	0.08414	0.49276 0.08728	0.41359 0.02343	0.19701 0.02230	0.10987 0.02205	4.28713 0.05860	2.45277 0.12129	0.34946 0.21366
OGLE-LMC-RRLYR-13862	797	1.23480	0.06661	0.82504 0.05998	0.54294 0.01337	0.37191 0.01263	0.21980 0.01212	4.01833 0.02609	2.16446 0.04203	0.06862 0.06829
OGLE-LMC-RRLYR-23324	309	0.81679	0.06638	0.76751 0.09538	0.55410 0.02940	0.33626 0.02778	0.23924 0.02675	4.21244 0.05588	2.51381 0.09486	0.49538 0.13684
OGLE-LMC-RRLYR-01648	322	0.74707	0.05604	0.83052 0.06144	0.59520 0.02545	0.37631 0.02384	0.21983 0.02223	4.07143 0.04673	2.22625 0.07837	0.44934 0.13042
OGLE-LMC-RRLYR-07370	635	3.23408	0.09796	0.55133 0.17864	0.31618 0.01646	0.13971 0.01613	0.06720 0.01585	4.16315 0.05235	1.79507 0.11525	5.21046 0.23776

4 DETERMINATION OF PHYSICAL PARAMETERS

One of the major constraints in deriving the physical parameters of RRL stars from I -band data is that most of the empirical relations connecting the Fourier parameters and the physical parameters are derived from the V -band RRL light curves. However, the huge RRab data obtained from various automated surveys and space missions are not limited to the Cousins V -band (Udalski et al. 1997; Woźniak et al. 2004). It is, therefore, quite natural to look for some interrelations between these parameters obtained from a considerable number of well-sampled light curves, both in the V band as well as any other photometric band like the I -band. In the literature, there are several instances, where the Fourier parameters in different bands are scaled to

corresponding values in the standard V -band in order to make use of the useful empirical relations. For example, the Fourier phase parameter values ϕ_{31} for the Northern Sky Variability Survey (NSVS) photometric system were calibrated to the standard Johnson V photometric system using the 55 well observed RRab stars which had the compiled values of ϕ_{31} in the V -band (Kinemuchi et al. 2006). Deb & Singh (2010) also derived interrelations between various parameters of the RRL light curves in the V and I -band with highly accurate complementary light curves in the literature in order to derive the various physical parameters of the SMC RRL stars. Nemeč et al. (2011) also used the V -band empirical relationships between the Fourier parameters and the physical parameters in order to derive the various properties of the RRab stars observed with Kepler, by noting

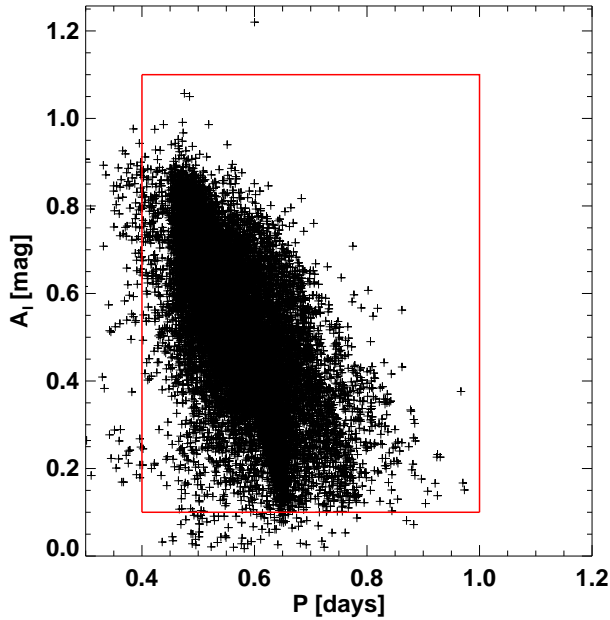


Figure 4. Period-Amplitude diagram for 17,693 stars in the OGLE database. The retained 17,092 RRab stars filtered through the selection criteria on period, amplitude and mean magnitude lie in the inner rectangle.

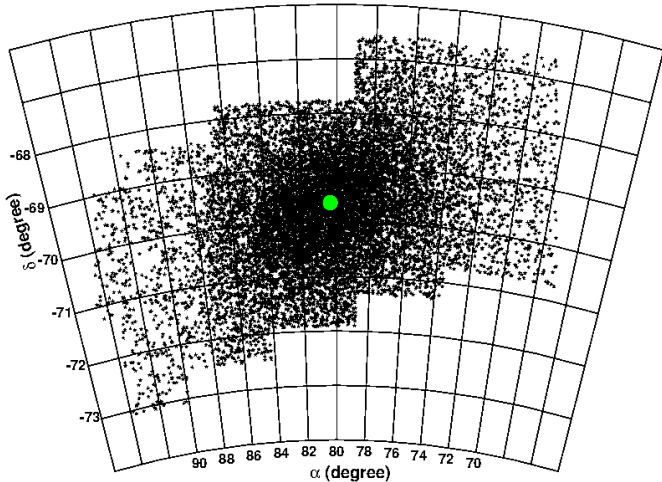


Figure 5. Equatorial coordinates (α, δ) of the selected sample of 13,095 RRab stars of the LMC. The filled circle denotes the position of the centroid $(\alpha_0, \delta_0) = (80^\circ.35, -69^\circ.65)$.

that the two broad photometric band filters Kp and V give similar results. For determination of RRab metallicities of LMC, Wagner-Kaiser & Sarajedini (2013) used the V -band amplitude obtained from the I -band amplitude given in the OGLE-III catalog through theoretical modeling.

Since the I -band light curves of the OGLE catalog have large number of data points as compared to the V -band light curves, the accuracy of the the Fourier parameters and hence the determined physical parameters is expected to be considerably higher. In the following section, we discuss the

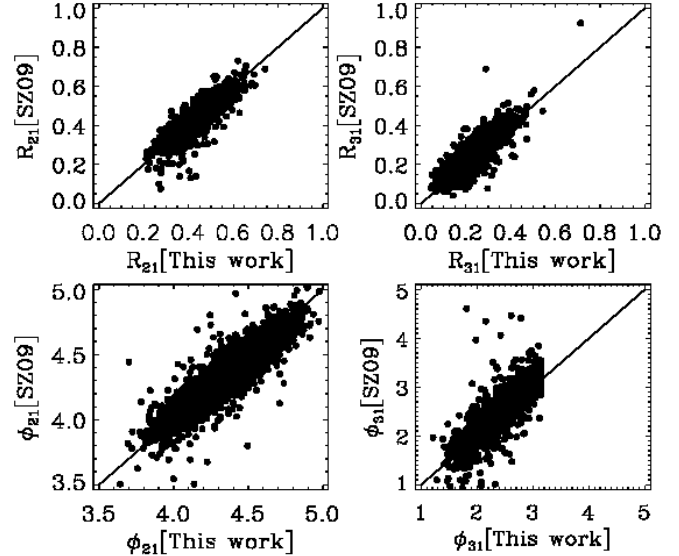


Figure 6. A comparison of the Fourier parameters R_{21} , R_{31} , ϕ_{21} , ϕ_{31} of 13,095 stars from Soszyński et al. (2009) and the present study.

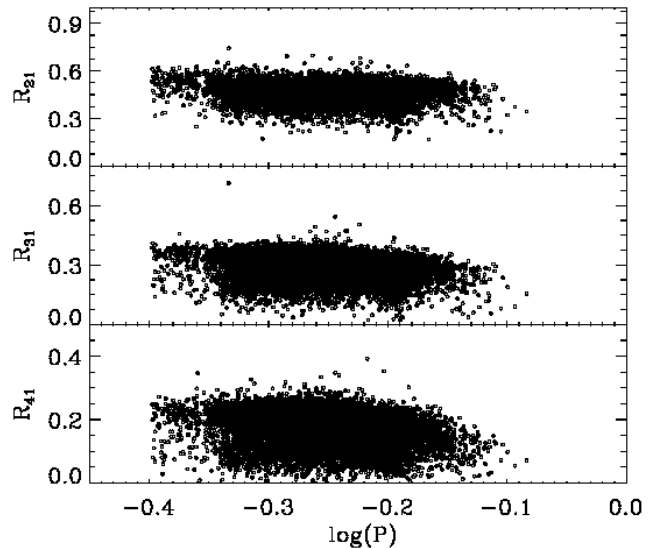


Figure 7. Fourier amplitude ratios R_{21} , R_{31} and R_{41} as a function of $\log(P)$ for the I -band data.

determination of physical parameters such as metallicities ($[Fe/H]$) and absolute magnitudes (M_V) of RRab stars selected from the OGLE-III catalog for the present study.

4.1 $[Fe/H]$ determinations

With the recent surge in the ground based photometric surveys and advent of space missions such as CoRoT and Kepler, an unprecedented pool of highly accurate and precise RRL light curve data has become available. The determination of metallicities of a large number of variable RRL stars from the photometric light curves has been possible through

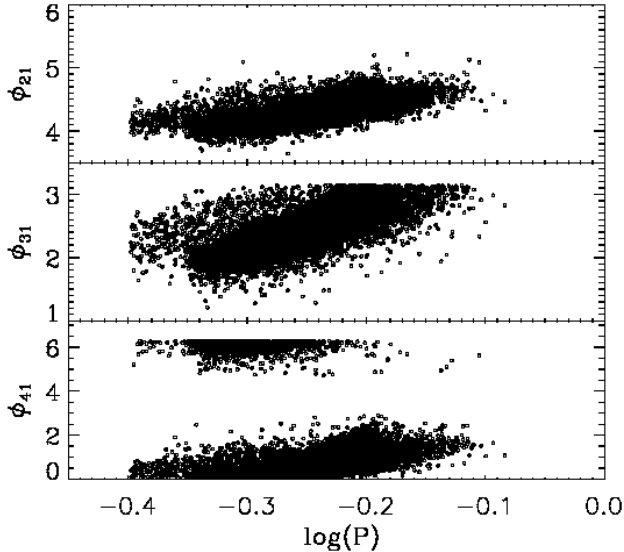


Figure 8. Fourier phase parameters ϕ_{21} , ϕ_{31} and ϕ_{41} as a function of $\log(P)$ for the I -band data.

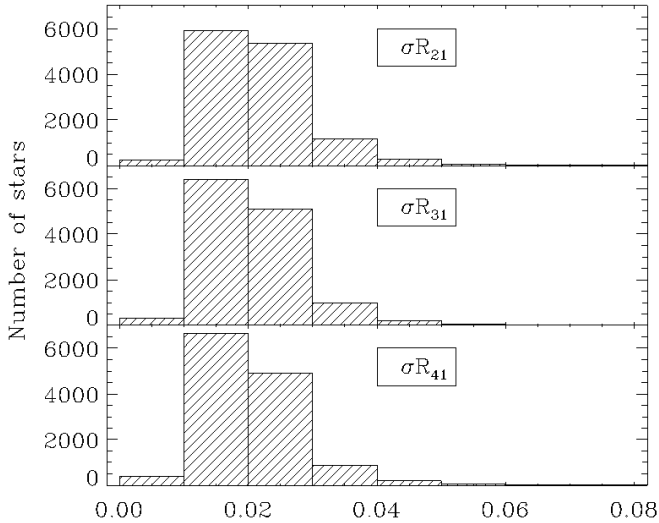


Figure 9. Histogram plot of the distribution of standard errors in R_{21} , R_{31} and R_{41} for the I -band data.

the use of various empirical relations between the metallicity and light curve parameters (Jurcsik & Kovacs 1996; Sandage 2004; Smolec 2005). This is a fast and cheaper alternative to the more accurate spectroscopic determinations. Numerous studies in the literature reveal the fact that the parameters determined from these empirical relations may not give consistent results for individual stars when compared with spectroscopic determinations but, nevertheless, prove to be useful when used for large homogeneous samples. For example, in order to examine whether there exists a metallicity gradient along the radial distance from the centre of a galaxy, the photometrically determined metallicities from a large number of RRL stars may provide a clue to the

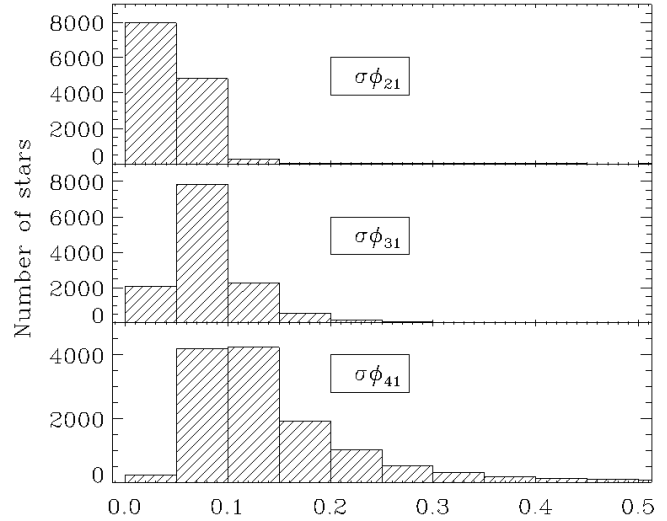


Figure 10. Histogram plot of the distribution of standard errors in ϕ_{21} , ϕ_{31} and ϕ_{41} for the I -band data.

answer. They also allow for a comparative study of metallicities among different clusters/galaxies.

The metallicities of the sample of RRab stars in the present study were determined using the empirical relations available in the literature. These empirical relations predict the period-metallicity relationship through the parameters like amplitude, color, rise time and Fourier phase parameter ϕ_{31} . These empirical period-metallicity relations were made on the basis of the fact that these light curve parameters vary with the period within the instability strip (Sandage 2004).

We start with the metallicity determinations using the relation of Jurcsik & Kovacs (1996, hereafter JK96). The JK96 $[Fe/H] - P - \phi_{31}$ relation is one of the highly used relations for metallicity determinations. However, the relation cannot be applied for the estimation of $[Fe/H]$ in peculiar stars, such as Blazhko variables and highly evolved stars. In order to select a clean sample of RRab stars having ‘normal-looking’ light curves, JK96 introduced a compatibility test for identifying ‘peculiar’ stars quantified by the deviations parameter D_F . This is defined as

$$D_F = \frac{F_{obs} - F_{calc}}{\sigma_{F_{obs}}}, \quad (3)$$

where F_{obs} is the observed value of a given parameter, F_{calc} is the predicted value from other observed parameters and σ_F is the corresponding deviation of various correlations as listed in Table 6 of JK96. We have used the compatibility test based on ϕ_{31} . For the I -band data, we have used a cut-off limit of $D_F = 5$ leaving us with clean sample of 13,095 RRab stars for the determination of $[Fe/H]$ and for further analysis.

The empirical relation of JK96 connecting ϕ_{31} in the V -band, period P and the metallicity $[Fe/H]$ is given by

$$[Fe/H]_{JK} = -5.038 - 5.394 P + 1.345 \phi_{31}, \quad \sigma = 0.14. \quad (4)$$

To use this relation, we need to convert the I -band Fourier parameters to those in the V -band. In order to make use of

Eqn. 4, we use the following relation (Deb & Singh 2010)

$$\phi_{31}^V = (0.436 \pm 0.075) + (0.568 \pm 0.030)\phi_{31}^I. \quad (5)$$

The above relation was obtained from a highly accurate set of light curves of 29 RRAb variables by Deb & Singh (2010). The relation exhibits a correlation coefficient of $R^2 = 0.912$, where $R^2 = 1$ corresponds to a perfect correlation. It should be noted that the above relation was obtained for the cosine Fourier decomposition. A factor of π has to be added or subtracted in order to convert ϕ_{31} from cosine to sine series or vice-versa. The metallicity values obtained from Eqn. 4 is in Jurcsik & Kovacs (1996) scale, which can be transformed into the metallicity scale of Zinn & West (1984, hereafter, ZW84) using the relation from Jurcsik (1995):

$$[Fe/H]_I = \frac{[Fe/H]_{JK} - 0.88}{1.431}. \quad (6)$$

Using the *I*-band data and the corresponding metallicity values, Smolec (2005) obtained the following relation involving the period and the phase parameter ϕ_{31} using the sine series

$$[Fe/H]_S = -(3.142 \pm 0.636) - (4.902P \pm 0.375) + (0.824 \pm 0.104)\phi_{31}, \quad \sigma = 0.18. \quad (7)$$

The above relation given by Eqn. 7 is based on the metallicity scale of Jurcsik & Kovacs (1996), which is converted into the metallicity scale of ZW84 using Eqn. 6. Let the metallicity in this new scale be denoted by $[Fe/H]_{II}$ as follows:

$$[Fe/H]_{II} = \frac{[Fe/H]_S - 0.88}{1.431}. \quad (8)$$

Alcock et al. (2000) showed that the metallicities of RRAb stars are linked to the period P and *V*-band amplitude of the light through the following empirical relation

$$[Fe/H]_{III} = -2.6 - 8.85[\log(P) - 0.15A_V], \quad \sigma = 0.31 \quad (9)$$

where A_V is obtained from the following relation of Deb & Singh (2010)

$$A_V = 0.071(\pm 0.019) + 1.500(\pm 0.040)A_I. \quad (10)$$

Another estimate of $[Fe/H]$ can be obtained from $[Fe/H] - \log P - \phi_{31}$ relation of Sandage (2004) given by

$$[Fe/H]_{IV} = -6.025 - 7.012 \log P + 1.411\phi_{31}, \quad \sigma = 0.16. \quad (11)$$

The above relation is based on the cosine series. The intercept term in this relation has an uncertainty of 0.023, ϕ_{31} and $\log P$ have respective uncertainties of 0.014 and 0.071. It should be noted that the determined metallicity values using the above relations do not yield the same result on a star-to-star basis. We have fitted a three parameter Gaussian function to each metallicity distribution of the present sample of 13,095 RRAb stars. The following peak values are obtained: $\langle [Fe/H]_I \rangle = -1.57 \pm 0.12$ dex, $\langle [Fe/H]_{II} \rangle = -1.50 \pm 0.12$ dex, $\langle [Fe/H]_{III} \rangle = -1.67 \pm 0.18$ dex and $\langle [Fe/H]_{IV} \rangle = -1.57 \pm 0.20$ dex. In the determination of these peak values, a constant bin size of 0.2 dex has been used. Fig. 11 shows the metallicity distribution of 13,095 RRAb stars obtained using the above four empirical relations. A scatter plot of the metallicity values of 13,095 RRAb stars obtained using the Smolec (2005) is shown in Fig. 12 against the metallicity values using the JK96 relations after ϕ_{31}^I has been converted into the corresponding ϕ_{31}^V

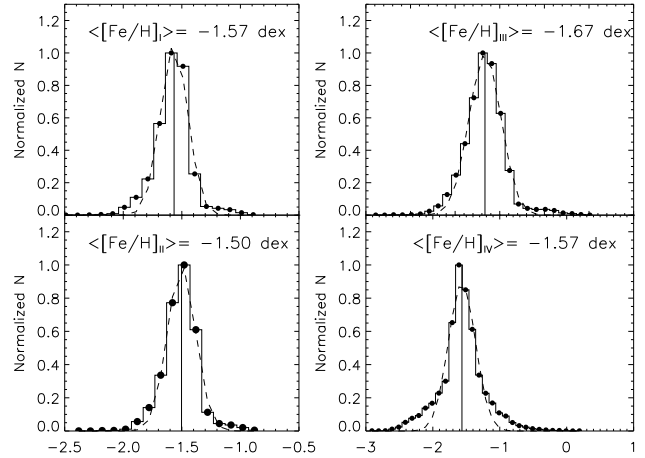


Figure 11. Metallicity distribution of 13,095 RRAb stars selected for the present analysis using the four empirical relations as described in the text.

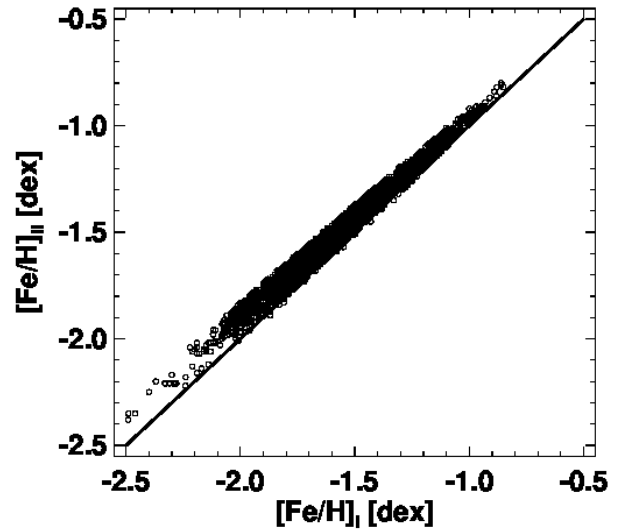


Figure 12. Comparison of metallicities of 13,095 stars determined using the Smolec (2005) relation for the *I*-band ($[Fe/H]_{II}$) and those determined from the JK96 relation using the calibration relation of Eqn. 5 in the present study ($[Fe/H]_I$).

using the calibration relation given by Eqn. 5. The metallicity values obtained using the Smolec (2005) relation are on an average higher by 0.07 dex. We adopt the metallicity values $[Fe/H]_I$ in the analysis that follows and denote these as $[Fe/H]$.

Fig. 13 shows the parameter space of ϕ_{31}^V versus P . An apparent random scatter of the data points is quite discernible. The scatter is in fact strongly correlated with the metallicity. The strong separation of three metallicity groups is quite evident from the figure. The segregation of data points on the $\phi_{31}^V - P$ diagram allows them to be divided into three metallicity groups, namely, *I*, *II* and *III* with metallicity values in the range $[Fe/H] \geq -1.35$ dex

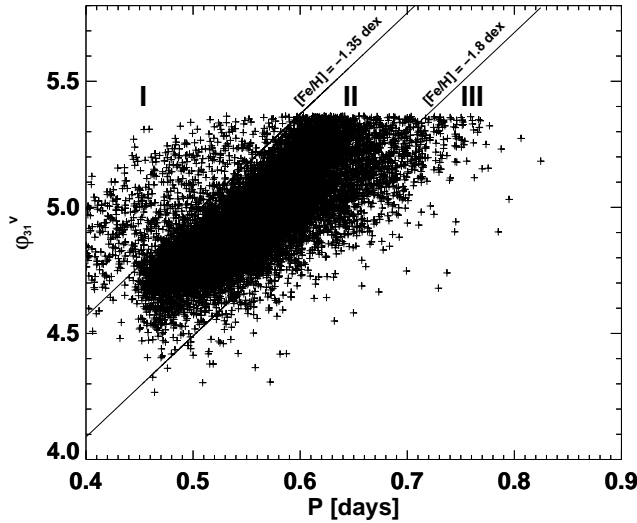


Figure 13. Representation of 13,095 stars on the $P - \phi_{31}$ plane. The diagram is clearly separated into three regions marked by *I*, *II* and *III* which correspond to the stars with $[Fe/H] \geq -1.35$ dex, $-1.80 < [Fe/H] < -1.35$ dex and $[Fe/H] \leq -1.80$ dex, respectively.

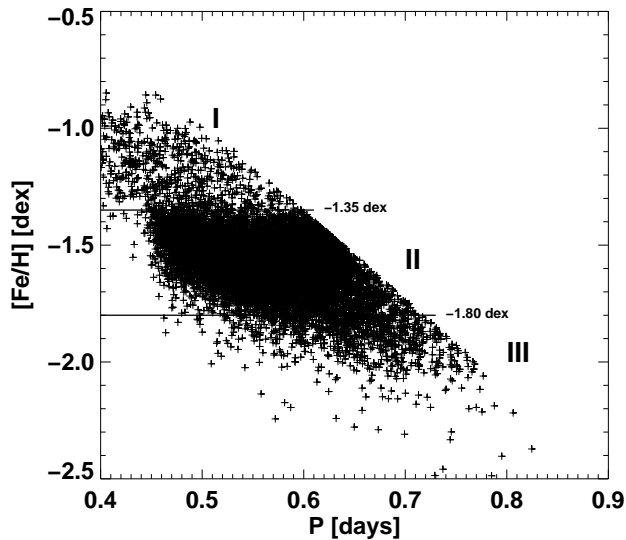


Figure 14. Representation of 13,095 stars on the $P - [Fe/H]$ plane. The three regions having three different metallicity groups as in Fig. 13 are marked by *I*, *II* and *III*, respectively.

(metal-rich), $-1.80 < [Fe/H] < -1.35$ dex (metal-poor), and $[Fe/H] \leq -1.80$ dex (extremely metal-poor), respectively as obtained from the data. Fig. 14 shows the three groups in the $P - [Fe/H]$ plane. The number of stars in each of the groups *I*, *II* and *III* are 659, 11406 and 1030, respectively. The mean metallicities of these three groups are found to be -1.20 ± 0.12 dex (*I*), -1.57 ± 0.10 dex (*II*) and -1.89 ± 0.09 dex (*III*).

4.2 Absolute magnitudes and distances

The empirical relation to estimate the absolute magnitudes (M_V) of RRab stars in terms of the period (P) and the Fourier coefficients (A_1 and A_3) is given by Kovács & Walker (2001):

$$M_V = -1.876 \log P - 1.158A_1 + 0.821A_3 + K, \quad (12)$$

Using the distance modulus of 18.50 mag for the LMC (Freedman et al. 2001), Arellano Ferro et al. (2010) found $K = 0.41$. We use $K = 0.41$ in Eqn. 12 to estimate the absolute magnitude of 13,095 RRab stars of the LMC. Mean values of absolute magnitudes of the three metallicity groups are: 0.70 ± 0.08 mag (*I*), 0.59 ± 0.06 mag (*II*) and 0.49 ± 0.08 mag (*III*). The absolute magnitudes are converted to luminosities using the standard relation

$$\log \left(\frac{L}{L_\odot} \right) = (4.75 - (M_V + BC_V)). \quad (13)$$

Here, we use $M_{bol}(\text{Sun}) = +4.75$. The bolometric correction (BC_V) is calculated using the equation (Sandage & Cacciari 1990)

$$BC_V = 0.06 + 0.06[Fe/H]. \quad (14)$$

Once the absolute magnitudes of the RRL stars are obtained, the intensity-weighted mean magnitude ($\langle V \rangle$) were used to derive their distance moduli. The values of $\langle V \rangle$ have been calculated using Eqn. 15 of Deb & Singh (2010). The values of $\langle I \rangle$ were calculated following Saha & Hoessel (1990). Mean values of $\langle I \rangle$ for each of these groups are 19.07 ± 0.27 mag, 18.83 ± 0.24 mag and 18.22 ± 0.25 mag, whereas the corresponding mean values of $\langle V \rangle$ are 19.63 ± 0.27 mag, 19.39 ± 0.24 mag and 19.22 ± 0.25 mag, respectively.

In order to determine the interstellar extinction A_V , we use the following relation (Schlegel et al. 1998)

$$A_V = 3.24(E(V - I)/1.4), \quad (15)$$

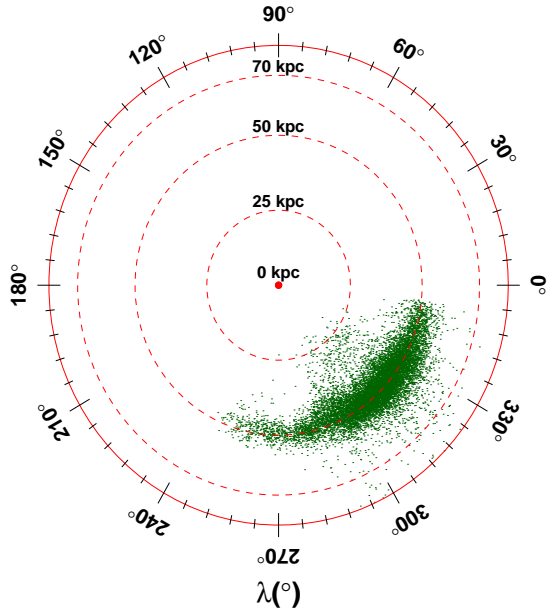
where the reddening values $E(V - I)$ are calculated from the LMC extinction map based on the OGLE-III RRL stars by Pejcha & Stanek (2009). Mean distances to each of the three metallicity groups are: 52.25 ± 6.20 kpc (*I*), 49.36 ± 5.30 kpc (*II*) and 47.87 ± 5.25 kpc (*III*). Table 3 shows the various parameters determined for the 13,095 RRab stars in this study. μ and D represent the distance modulus in mag and distance in kpc, respectively. Fig. 15 shows polar plot of the distance distribution of LMC RRab stars in ecliptic coordinates. The dashed lines are set at distances $D = 25, 50, 70$ kpc, respectively.

5 STRUCTURE OF THE LMC

The Cartesian coordinates corresponding to each star can be obtained using the $RA(\alpha)$, $Dec(\delta)$ and the distance D in kpc. Let us consider the Cartesian coordinate system (x, y, z) which has the origin at the center of the LMC at $(\alpha, \delta, D) = (\alpha_0, \delta_0, D_0)$. The z -axis is pointed towards the observer, the x -axis is antiparallel to the α -axis and the y -axis is parallel to the δ -axis. D_0 is the distance between the center of the LMC and the observer while D is the observer-source distance and (α_0, δ_0) are the equatorial coordinates of

Table 3. Various parameters extracted from Fourier coefficients for 13,095 RRAb variables. Errors represent the uncertainties in the Fourier parameters. The complete table is available in the electronic version of this paper.

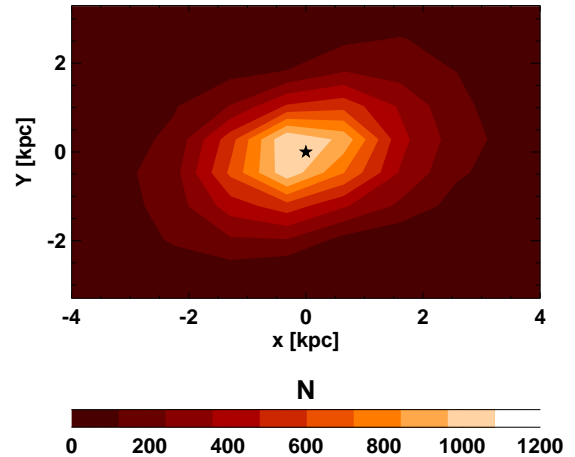
OGLE ID (1)	[Fe/H] [dex] (2)	M_V [mag] (3)	$\log(L/L_\odot)$ (4)	$\langle I \rangle$ [mag] (5)	$\langle V \rangle$ [mag] (6)	μ [mag] (7)	D [kpc] (8)
OGLE-LMC-RRLYR-23488	-1.09± 0.11	0.80±0.008	1.58± 0.00	19.12	19.68	18.61± 0.04	52.61± 0.40
OGLE-LMC-RRLYR-20444	-1.17± 0.12	0.81±0.009	1.58± 0.00	19.33	19.89	18.66± 0.07	53.98± 0.74
OGLE-LMC-RRLYR-17769	-1.12± 0.09	0.76±0.003	1.60± 0.00	19.06	19.61	18.53± 0.09	50.93± 0.92
OGLE-LMC-RRLYR-21760	-0.96± 0.13	0.80±0.010	1.58± 0.01	19.48	20.03	18.72± 0.06	55.52± 0.63
OGLE-LMC-RRLYR-11295	-1.15± 0.13	0.74±0.007	1.61± 0.00	19.10	19.66	18.69± 0.04	54.83± 0.41
OGLE-LMC-RRLYR-03670	-0.98± 0.14	0.84±0.006	1.56± 0.00	19.34	19.89	18.76± 0.07	56.40± 0.84
OGLE-LMC-RRLYR-13862	-1.13± 0.09	0.78±0.004	1.59± 0.00	19.12	19.68	18.69± 0.07	54.63± 0.77
OGLE-LMC-RRLYR-23324	-0.95± 0.12	0.79±0.009	1.58± 0.00	19.23	19.78	18.68± 0.04	54.51± 0.45
OGLE-LMC-RRLYR-01648	-1.10± 0.11	0.79±0.008	1.58± 0.00	19.19	19.74	18.68± 0.04	54.49± 0.40
OGLE-LMC-RRLYR-07370	-1.33± 0.13	0.78±0.004	1.60± 0.00	19.13	19.68	18.45± 0.18	48.99± 1.75
OGLE-LMC-RRLYR-20673	-1.21± 0.13	0.75±0.009	1.61± 0.00	19.17	19.73	18.68± 0.06	54.36± 0.64

**Figure 15.** Polar plot of the distance distribution of LMC RRAb stars in ecliptic coordinates. The dashed lines are set at distances $D = 25, 50, 70$ kpc, respectively.

the center of the LMC. The (x, y, z) coordinates are obtained using the transformation equations (van der Marel & Cioni 2001; Weinberg & Nikolaev 2001):

$$\begin{aligned}
 x &= -D \sin(\alpha - \alpha_0) \cos \delta, \\
 y &= D \sin \delta \cos \delta_0 - D \sin \delta_0 \cos(\alpha - \alpha_0) \cos \delta, \\
 z &= D_0 - D \sin \delta \sin \delta_0 - D \cos \delta_0 \cos \alpha - \alpha_0 \cos \delta.
 \end{aligned}
 \tag{16}$$

The coordinate system of the LMC disk (x', y', z') is the same as the orthogonal system (x, y, z) , except that it is rotated around the z -axis by position angle θ counterclockwise and around the new x -axis by the inclination angle i clockwise. The coordinate transformations can be written as

**Figure 16.** Two dimensional number density of 13,095 RRAb stars is shown as a contour map. The star symbol denotes the location of the centroid for the present sample.

(van der Marel & Cioni 2001; Weinberg & Nikolaev 2001):

$$\begin{aligned}
 x' &= x \cos \theta + y \sin \theta, \\
 y' &= -x \sin \theta \cos i + y \cos \theta \cos i - z \sin i, \\
 z' &= -x \sin \theta \sin i + y \cos \theta \sin i + z \cos i.
 \end{aligned}$$

The two dimensional density contours of the distribution of the LMC RRAb stars are shown in Fig. 16. The star symbol denotes the location of the centroid of the present sample.

5.1 Vertical distribution of the stars

In this section, we study the vertical $|z|$ distribution of the LMC RRAb stars. In order to see how the metal poor and metal rich RRAb stars are distributed in the vertical, we divide the stars into three metallicity groups, viz, *I*, *II* and *III* as described in section 4.1. We further use a bin size of 1 kpc and count the number of stars falling in each bin. The resulting distribution of metallicity group *I* (metal rich

stars) is shown in Fig. 17. From the figure, we can see that the stars of this group are mainly distributed upto a distance of ~ 10 kpc, after which the distribution becomes uniform. The number of metal rich stars lying below $z = 10$ kpc are 639 ($\sim 97.0\%$) while lying above it are 20 ($\sim 3.0\%$) only, out of a total of 659. On the other hand, the distribution of the RRab stars belonging to metallicity groups *II* (metal poor) and *III* (extremely metal poor) are shown in Fig. 18. Upto a distance of 10 kpc, the number of stars belonging to the groups *II* and *III* are 11,015 and 973, out of a total of 11,406 and 1030, respectively. These account for 96.57% and 94.47%, respectively of the total. The number of stars in each of these groups decrease with increasing distance from the galactic plane. Also, it can be seen that number of metal poor stars are very large as compared to the metal rich stars within a distance of 10 kpc. It is also found that more than 94% (12,340) of the total number of RRab stars lie within $|z| = 10$ kpc. Less than 10% of the RRab stars are located beyond a $|z|$ distance of 10 kpc with majority of them being metal poor ($[Fe/H] < -1.35$ dex). This implies that the RRLs in the LMC belong to two different structures, one with smaller scale height tracing the disk and the other with larger scale height tracing the inner halo of the LMC.

Since a majority of the metal poor RRab stars lie within $|z| = 10$ kpc which traces the disk, we may conclude that the disk of the LMC has been formed much earlier than the extended halo of the LMC. This confirms the findings of Subramaniam & Subramanian (2009) that RRLs in the inner LMC belong to two different populations tracing the disk and the inner halo. The spatial distribution of the LMC RRab stars and their metallicities indicate that the majority of the old and metal-poor LMC field stars lie in a disk and not in a spheroid. Fig. 19 shows the $|z|$ distribution of all RRab stars of the LMC selected in the present study. The radial number density profile of all the RRab stars as a function of galactocentric distance is shown in Fig. 20. The radial number density profile is obtained by projecting the radial number density of RRabs in concentric rings around the centroid of the LMC.

5.2 Inclination angle (i) and position angle of the line of nodes (θ_{lon})

Once we have the distribution of RRab distances as determined above, we apply the least square plane fitting method and the method of principal axes transformation using the moment of inertia tensor in order to get an estimate of the viewing angles of the LMC. In order to obtain the viewing angles of the LMC disk, viz., the inclination i and position angle of the line of nodes θ_{lon} , the distances are projected on coordinate axes (x, y, z). Once the x, y and z coordinates are obtained using Eqn. 16, we apply a plane fit equation of the form (Nikolaev et al. 2004)

$$z_i = ax_i + by_i + c, \quad i = 1, 2, \dots, N. \quad (17)$$

The fit to z_i is obtained as a function of (x_i, y_i) . From the coefficients of the plane fit solution, the inclination (i) and position angle of the line of nodes (θ) can be calculated using

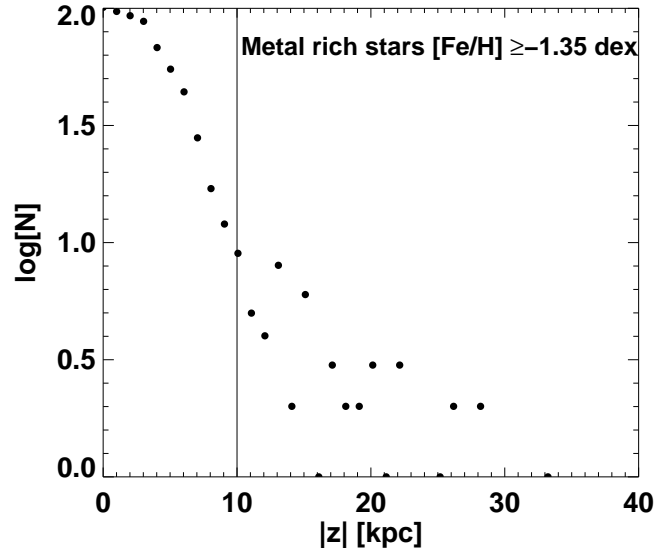


Figure 17. Distribution of metal rich ($[Fe/H] \geq -1.35$ dex) RRab stars of the LMC as a function of vertical $|z|$ distance from the galactic plane.

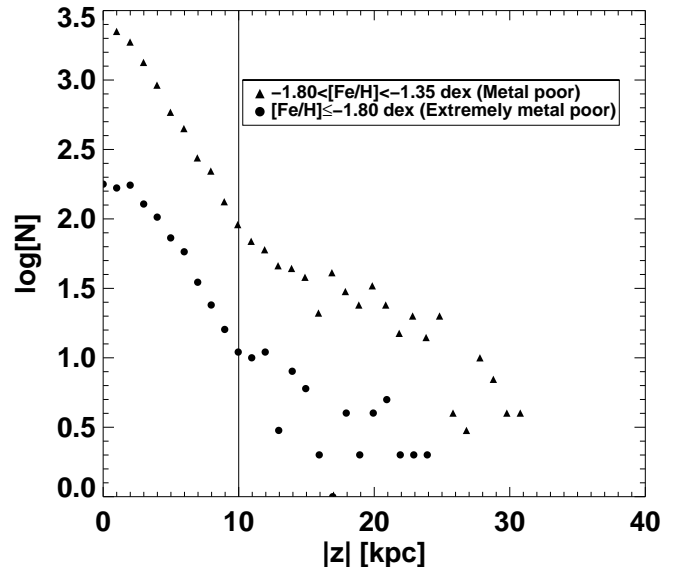


Figure 18. Distribution of metal poor ($-1.80 < [Fe/H] < -1.35$ dex) and extremely metal rich ($[Fe/H] \leq -1.80$ dex) RRab stars of the LMC as a function of vertical $|z|$ distance from the galactic plane.

the following formula (Nikolaev et al. 2004)

$$i = \arccos\left(\frac{1}{\sqrt{(1+a^2+b^2)}}\right), \quad (18)$$

$$\theta = \arctan\left(-\frac{a}{b}\right) + \text{sign}(b)\frac{\pi}{2}. \quad (19)$$

The plane fitting procedure has been carried out using $|z| = 10$ kpc (12,340 RRab stars), taken as the boundary of the LMC disk obtained from the vertical z distribution of the metal rich RRab stars. The values obtained for the LMC disk are $i = 36^\circ.43$ and $\theta_{lon} = 149^\circ.08$.

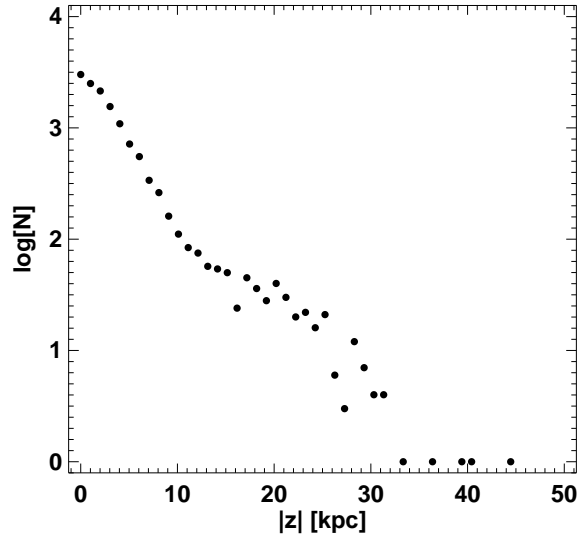


Figure 19. Distribution of all RRab stars of the LMC as a function of vertical $|z|$ distance from the galactic plane.

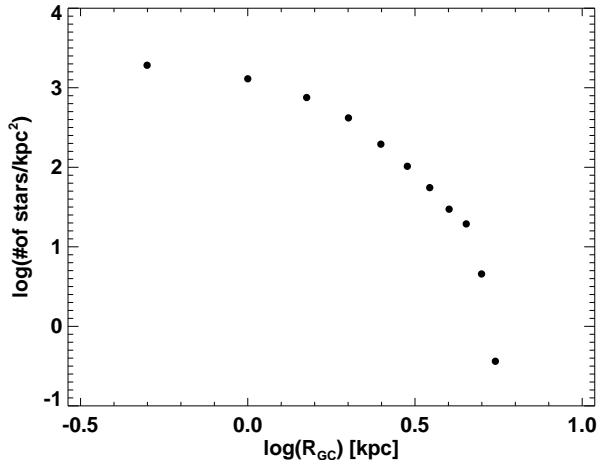


Figure 20. Radial number density distribution of 13,095 RRab stars as a function of galactocentric distance in logarithmic scale.

Now, we model the observed population of the RRab stars in LMC by a triaxial ellipsoid upto a $|z|$ distance of 10 kpc. The properties of the ellipsoid can be obtained from the moment of inertia tensor using the principal axes transformation. In order to apply the principal axes transformation, we first construct the covariance matrix (inertia tensor) from the $[x(i), y(i), z(i), i = 1, \dots, N]$ distribution of the RRab stars. To construct the covariance matrix, we first determine the centroid of the distribution using Karnesky et al.

(2007)

$$\begin{aligned}\bar{x} &= \sum_{i=1}^N x(i)/N, \\ \bar{y} &= \sum_{i=1}^N y(i)/N, \\ \bar{z} &= \sum_{i=1}^N z(i)/N,\end{aligned}\tag{20}$$

and then construct the covariance matrix called the moment of inertia tensor as (Karnesky et al. 2007; Huang 2011)

$$I = \begin{bmatrix} I_{xx} & -I_{xy} & -I_{xz} \\ -I_{yx} & I_{yy} & -I_{yz} \\ -I_{zx} & -I_{zy} & I_{zz} \end{bmatrix},\tag{21}$$

where

$$\begin{aligned}I_{xx} &= \Theta_{yy} + \Theta_{zz}, \\ I_{yy} &= \Theta_{xx} + \Theta_{zz}, \\ I_{zz} &= \Theta_{xx} + \Theta_{yy}, \\ I_{xy} &= I_{yx} = \Theta_{xy}, \\ I_{xz} &= I_{zx} = \Theta_{xz}, \\ I_{yz} &= I_{zy} = \Theta_{yz},\end{aligned}\tag{22}$$

and

$$\begin{aligned}\Theta_{xx} &= \frac{1}{N} \sum_{i=1}^N (x(i) - \bar{x})^2, \\ \Theta_{yy} &= \frac{1}{N} \sum_{i=1}^N (y(i) - \bar{y})^2, \\ \Theta_{zz} &= \frac{1}{N} \sum_{i=1}^N (z(i) - \bar{z})^2, \\ \Theta_{xy} &= \frac{1}{N} \sum_{i=1}^N (x(i) - \bar{x})(y(i) - \bar{y}), \\ \Theta_{xz} &= \frac{1}{N} \sum_{i=1}^N (x(i) - \bar{x})(z(i) - \bar{z}), \\ \Theta_{yz} &= \frac{1}{N} \sum_{i=1}^N (y(i) - \bar{y})(z(i) - \bar{z}).\end{aligned}\tag{23}$$

When the axes of the coordinate frame (x, y, z) are selected such that $I_{xy} = I_{xz} = I_{yz} = 0$, we have the principal axes of inertia of the system. The corresponding moments of inertia I_{xx}, I_{yy} , and I_{zz} are the principal moments of inertia (Huang 2011). It can be seen that the covariance matrix I is real and symmetric. Let the matrix I have the eigenvalues ($\lambda_1 > \lambda_2 > \lambda_3$) and $\{\vec{e}_1, \vec{e}_2, \vec{e}_3\}$ be the corresponding eigenvectors normalized to unity. In order to obtain the principal axes of the coordinate frame, we need to diagonalize the symmetric covariance matrix. The eigenvectors of the matrix I can be used to form another matrix T such that the matrix $T^{-1}IT$ is a diagonal matrix. The diagonal elements of the diagonal matrix are the eigenvalues of I (Press et al. 2002; Tang 2006; Karnesky et al. 2007). Here T is the matrix formed with the eigenvectors of I as the column vectors. It can be shown that the matrix T is an orthogonal matrix and diagonalizes the covariance matrix T (Press et al. 2002; Tang 2006; Huang

2011). The new coordinate axes in which the matrix I is diagonal are known as the principal axes (Press et al. 2002; Tang 2006). The diagonalization

$$I' = T^{-1}IT = T^\dagger IT, \quad (24)$$

yields

$$I' = \begin{bmatrix} \lambda_1 & 0 & 0 \\ 0 & \lambda_2 & 0 \\ 0 & 0 & \lambda_3 \end{bmatrix}. \quad (25)$$

The three eigenvalues ($\lambda_1 > \lambda_2 > \lambda_3$) correspond to non-zero diagonal terms of the inertia tensor in the new coordinate system and are called the principal moments of inertia of the system. The eigenvectors corresponding to the three eigenvalues represent three orthogonal axes in the new coordinate system and are called the principal axes of the new coordinate system (Press et al. 2002; Tang 2006). The transformation matrix or the rotation matrix which carries out the transformation $T : R^3 \rightarrow R^3$ is given by

$$T(\vec{e}) = \vec{e}',$$

where $\vec{e} = (e_1, e_2, e_3)^T$ and $\vec{e}' = (e'_1, e'_2, e'_3)^T$, where \vec{e}_i, \vec{e}'_i are the basis vectors in the Cartesian coordinate systems (x, y, z) and the new coordinate system, respectively. The basis vectors \vec{e}_i and \vec{e}'_i are related by an orthogonal tensor \mathbf{T} through the equations given below

$$\vec{e}'_i = \mathbf{T}\vec{e}_i = \sum_{j=1}^3 T_{ij}\vec{e}_j \quad (26)$$

That is,

$$\vec{e}'_1 = T_{11}\vec{e}_1 + T_{12}\vec{e}_2 + T_{13}\vec{e}_3, \quad (27)$$

$$\vec{e}'_2 = T_{21}\vec{e}_1 + T_{22}\vec{e}_2 + T_{23}\vec{e}_3, \quad (28)$$

$$\vec{e}'_3 = T_{31}\vec{e}_1 + T_{32}\vec{e}_2 + T_{33}\vec{e}_3, \quad (29)$$

$$(30)$$

where

$$T_{ij}T_{kj} = T_{ji}T_{jk} = \delta_{ik} \Rightarrow TT^\dagger = TT^\dagger = 1 \quad (31)$$

It may be noted that

$$T_{ij} = \cos(\vec{e}_i, \vec{e}'_j). \quad (32)$$

The matrix formed from these direction cosines, i.e., the matrix

$$\begin{bmatrix} T_{11} & T_{21} & T_{31} \\ T_{12} & T_{22} & T_{32} \\ T_{13} & T_{23} & T_{33} \end{bmatrix}, \quad (33)$$

is called the transformation matrix between $\{\vec{e}_1, \vec{e}_2, \vec{e}_3\}$ and $\{\vec{e}'_1, \vec{e}'_2, \vec{e}'_3\}$. The transformation matrix or the rotation matrix consists of the eigenvectors of I as the column vectors. The transformation matrix T describes the spatial directions or the orientation of the ellipsoid with respect to the local coordinate system (x, y, z) (Press et al. 2002; Tang 2006; Karnesky et al. 2007).

Applying the above method to the distribution of the RRab stars in the coordinate system, we obtain the eigenvalues $\lambda_1 = 14.85, \lambda_2 = 13.46$ and $\lambda_3 = 2.92$. From the transformation matrix, we estimate the inclination angle and

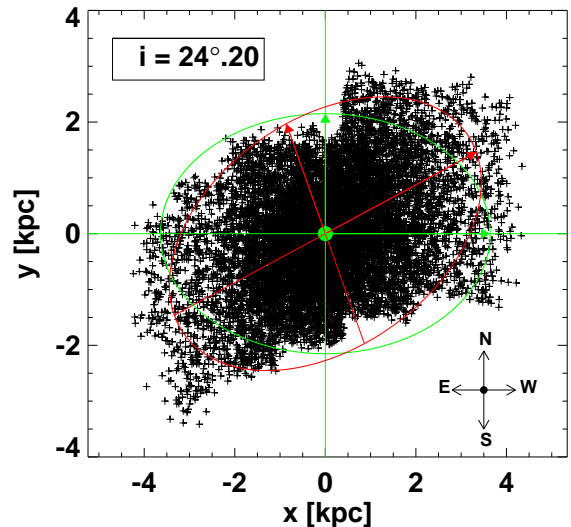


Figure 21. The value of the inclination angle as obtained from the principal axes transformation of the moment of inertia tensor is shown. The filled green circle denotes the origin (0,0) of the distribution. N, E, S, W represent the north, east, south and west directions, respectively.

position angle of the line of nodes as $24^\circ.20$ and $176^\circ.01$ respectively. The lengths of the semi-axes (S_i) of the best-fit ellipsoid are obtained using (Karnesky et al. 2007)

$$S_i = \sqrt{\frac{5}{2}(\lambda_j + \lambda_k - \lambda_i)}, \quad \text{for } i \neq j \neq k. \quad (34)$$

where $S_1 > S_2 > S_3$ are the major-axis and two minor axes, respectively. The lengths of the axes are estimated as: $S_1 = 7.97$ kpc, $S_2 = 3.28$ kpc and $S_3 = 1.96$ kpc. The eccentricity of the LMC disk is found to be $e = 0.41$. The value of the inclination angle as determined from the best-fit ellipsoid in the (x, y) - plane is shown in Fig. 21. The best-fit ellipsoid to the three-dimensional (x, y, z) distribution is shown in Fig. 22.

5.3 Dependence of viewing angles on the choice of the LMC center

In this section, we study the effect of the choice of the LMC center on the determination of the viewing angles of the LMC disk. The LMC does not have a unique, well-defined viewing angle (van der Marel & Cioni 2001). Thus, the choice of the LMC center taken as the centroid in this study is to some extent arbitrary. However, we find that this has no influence on the accuracy of the results obtained. It does not lead to statistically different results for the best fitting viewing angles (i, θ_{lon}). In order to corroborate this fact, we consider the following five choices of the coordinate origin: (1) optical center, $(\alpha_0, \delta_0) = (79^\circ.91, -69^\circ.45, \text{J2000})$ from de Vaucouleurs & Freeman (1972), (2) center obtained from the distribution of novae, $(\alpha_0, \delta_0) = (80^\circ.07, -69^\circ.06, \text{J2000})$ from van den Bergh (1988) (3) center defined by *HI* rotation map, $(\alpha_0, \delta_0) = (79^\circ.4, -69^\circ.03, \text{J2000})$ from Kim et al. (1998) (4) center of carbon stars outer isopleths, $(\alpha_0, \delta_0) = (82^\circ.25, -69^\circ.5, \text{J2000})$ from van der Marel & Cioni (2001)

Table 4. Estimates of the viewing angles of the LMC obtained in this study for various choices of the LMC center in the reference with different types of tracers used given below. The viewing angle parameters in this study have been estimated using the principal axes transformation method

Reference	i	θ_{lon}	Tracers used
de Vaucouleurs & Freeman (1972)	24°.62	177°.16	Yellow light isophotes
van den Bergh (1988)	23°.50	175°.70	Novae
Kim et al. (1998)	25°.24	176°.38	HI
van der Marel & Cioni (2001)	22°.43	175°.27	AGB stars
Nikolaev et al. (2004)	22°.25	175°.22	Cepheids
Centroid of the present sample	24°.20	176°.01	RRab stars

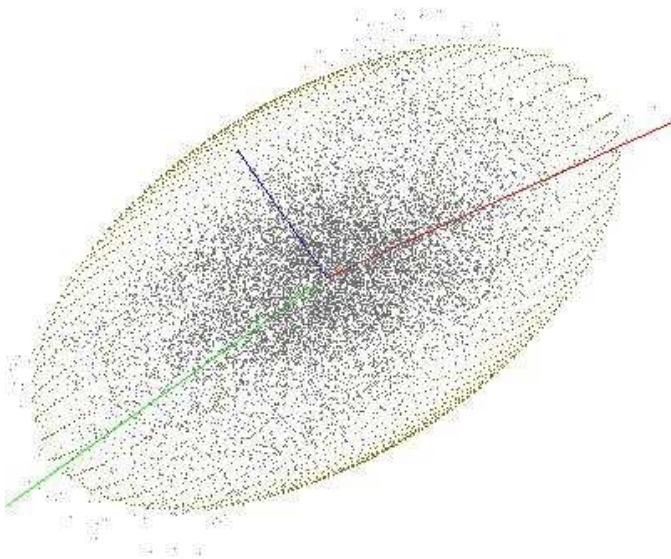


Figure 22. Best fit-ellipsoid obtained from the principal axis transformation of the moment of inertia tensor constructed from the x, y, z distributions of the RRab stars in the LMC.

and (5) geometric center obtained from Cepheids, $(\alpha_0, \delta_0) = (80^\circ.40, -69^\circ.00, \text{J2000})$ from Nikolaev et al. (2004). The parameters estimated using the above centers are listed in Table 4. We find that there are meagre changes in the best-fitted viewing angles (i, θ_{lon}) of the LMC disk on the choice of the origin.

5.4 Comparison with previous studies

There have been a number of previous studies on the geometrical parameters of the LMC using different tracers. Use of different types of tracers in order to disseminate the geometry yields wide range of values of the LMC disk inclination and the position angle of the line of nodes. As listed in the Table 3.5 of Westerland (1997), the inclination values of the LMC disk range from 27 to 48° and the position angles of

the line of nodes vary from 168 to 208° depending on the tracers used. The various other determinations of the LMC geometry obtained in the last 10 years are listed in Table 5.

A substantial number of studies which have attempted to find the viewing angles of the LMC disk using different types of tracers are tabulated in Table 1 of Subramanian & Subramanian (2013). The inclination values of the LMC disk in most of these studies are consistent with each other within the error bars. But, there is a lot of discrepancy when it comes to the determination of the position angles of the line of nodes. In this study of the LMC using the RRab stars from the OGLE-III database, we found an inclination $(i) = 24^\circ.20$ and position angle of the line of nodes $(\theta_{lon}) = 176^\circ.01$ from the method of principal axes transformation using the moment of inertia tensor. Using different types of tracers in the LMC, Weinberg & Nikolaev (2001) found the inclination of the LMC to the line of sight $i = 22$ to 29° and position angle of line of nodes $\theta_{lon} = 168$ to 173° obtained by fitting each population by two different models: a thin exponential disk and a spherical power-law model. The values of the viewing angles $(i, \theta_{lon}) = (24^\circ.20, 176^\circ.01)$ derived here from the principal axes transformation method are consistent with the values of Weinberg & Nikolaev (2001) and the values listed in Westerland (1997).

On the other hand, using the simple plane fitting procedure on the same dataset here yields $i = 36^\circ.43$ and $\theta_{lon} = 149^\circ.08$. The variation in the values of these geometrical parameters of the the LMC can be attributed to the highly complicated structure of the LMC as well as different methodology adopted in their determinations.

6 METALLICITY GRADIENT IN THE LMC

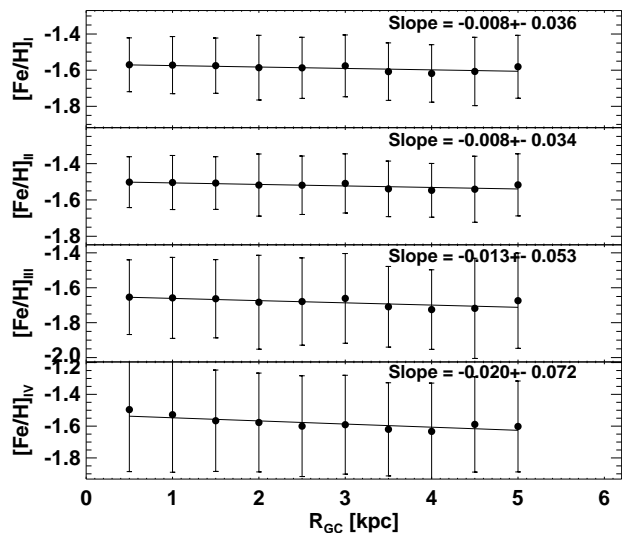
The presence of radial metallicity gradient in a galaxy provides clues to the presence of different stellar populations which might be related to its star formation history or to the accretion process by an external system (Bernard et al. 2008). There are some studies in the literature which hint at the presence of a metallicity gradient in the LMC (Cioni 2009; Feast et al. 2010; Wagner-Kaiser & Sarajedini 2013). On the other hand, some other studies claim that no such metallicity gradient ex-

Table 5. Various values of the viewing angle parameters (i, θ_{lon}) of the LMC disk obtained in the last 10 years

Reference	i	θ_{lon}	Tracers used
Nikolaev et al. (2004)	$30^\circ.7 \pm 1^\circ.1$	$151^\circ.0 \pm 02^\circ.4$	Cepheids
Persson et al. (2004)	$27^\circ.0 \pm 6^\circ.0$	$127^\circ.0 \pm 10^\circ.0$	Cepheids
Koerwer (2009)	$23^\circ.5 \pm 0^\circ.4$	$154^\circ.6 \pm 01^\circ.2$	Red clump stars
Subramanian & Subramaniam (2010)	$23^\circ.0 \pm 0^\circ.8$	$163^\circ.7 \pm 01^\circ.5$	Red Clump Stars (OGLE-III data)
Subramanian & Subramaniam (2010)	$37^\circ.4 \pm 2^\circ.3$	$141^\circ.2 \pm 03^\circ.7$	Red Clump Stars (MCPS data)
Subramanian & Subramaniam (2013)	$25^\circ.7 \pm 1^\circ.6$	$141^\circ.5 \pm 04^\circ.5$	Red Clump Stars (MCPS Infrared data)
Rubele et al. (2012)	$26^\circ.2 \pm 2^\circ.0$	$129^\circ.1 \pm 13^\circ.0$	Modeling of LMC disk plane
Haschke et al. (2012)	$32^\circ.0 \pm 4^\circ.0$	$114^\circ.0 \pm 13^\circ.0$	OGLE-III data (RRL stars)
Haschke et al. (2012)	$32^\circ.0 \pm 4^\circ.0$	$116^\circ.0 \pm 18^\circ.0$	OGLE-III data (Cepheids)
This work (Principal axes transformation method)	$24^\circ.20$	$176^\circ.01$	OGLE-III data (RRab stars)
This work (Plane fitting procedure)	$36^\circ.43$	$149^\circ.08$	OGLE-III data (RRab stars)

ists in the LMC (Grocholski et al. 2006; Carrera et al. 2011; Haschke et al. 2012; Piatti & Geisler 2013). These studies support the fact that the amount of gradient observed as a function of distance from the LMC center is very small compared to the error bars of the mean metallicity obtained as a function of distance bins from the center (Grocholski et al. 2006; Carrera et al. 2011; Haschke et al. 2012; Piatti & Geisler 2013). More recently, an extensive study based on the metallicities obtained from the age-metallicity relation of 21 LMC fields consisting of 5.5 million stars indicates that there exists no metallicity gradient in the LMC (Piatti & Geisler 2013).

RRL stars provide an unique opportunity to measure the metallicity of old stellar populations and serve as a valuable means to identify the existence of any possible metallicity gradient in a galaxy. In order to examine the question of metallicity gradient in the LMC, we have resorted to the metallicity values of RRab stars obtained here using the four empirical relations as described in the section 4.1 as a function of the galactocentric distances (R_{GC}). Galactocentric distances were calculated following the method of Cioni (2009), taking into consideration the viewing angles of the LMC disk: the inclination ($i = 24^\circ.20$) and the position angle of the line of nodes $\theta_{lon} = 176^\circ.01$ as determined for RRab stars outlined above using the principal axes transformation method. Angular distances and position angle coordinates of all the RRab stars were computed using the equations given in van der Marel & Cioni (2001) considering the center of the LMC ($\alpha_{2000} = 5^h 21^m 24^s$ and $\delta_{2000} = -69^\circ 39'$) as origin determined for the present sample. Fig. 23 shows the weighted mean metallicity values computed using different empirical relations as a function of distance in bins of 0.5 kpc from the LMC center (Bevington & Robinson 2003). $[Fe/H]_I, [Fe/H]_{II}, [Fe/H]_{III}, [Fe/H]_{IV}$ denote the mean metallicity values in each bin computed as a function of distance using Eqs. 4, 8, 11, 9, respectively. Least square fits to the distance and the mean metallicity values with their estimated errors to each of the data sets yield slopes of -0.008 ± 0.036 dex kpc^{-1} , -0.008 ± 0.034 dex kpc^{-1} , -0.013 ± 0.053 dex kpc^{-1} and -0.020 ± 0.072 dex kpc^{-1} . Statistically, all these values correspond to no metallicity gradient. In the estimation of mean metallicity values in


Figure 23. Mean metallicity distribution of 13,095 RRab stars as a function of galactocentric distance in kpc with a bin size of 0.5 kpc. Mean metallicities in each bin has been obtained using the four empirical relations as described in the text.

each distance bin, we have ensured that the number of stars are greater than 10 for reliable statistics. Also, in the calculation of mean metallicity errors, we have taken into account the errors due to the uncertainties in the Fourier parameters and the systematic errors in each of the empirical relations. These two errors were added quadratically for each star in order to estimate the mean metallicity and its associated error in a distance bin. All the empirical relations for metallicity calculations do not show any significant metallicity gradient within the uncertainties, consistent with the results obtained by Grocholski et al. (2006), Carrera et al. (2011), Haschke et al. (2012) and Piatti & Geisler (2013), at least in the inner 6 kpc of the LMC. Fig. 24 shows the metallicity map of LMC RRab stars on a rectangular grid. To produce the (x, y) -map, the observed LMC area were binned on a (10×10) grid. The average values of the metal-

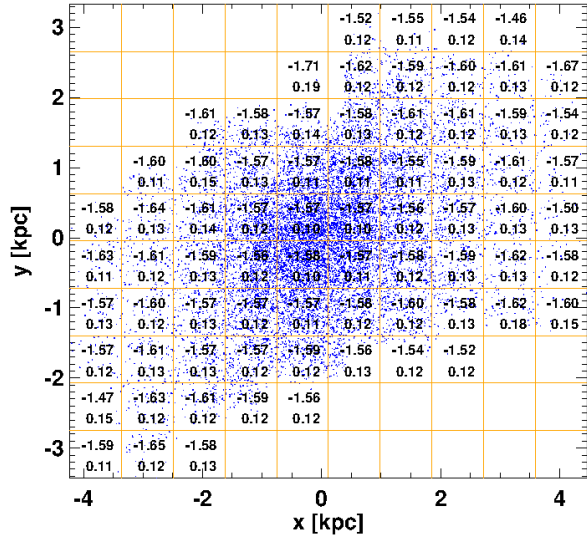


Figure 24. Metallicity distribution of 13,095 RRab stars in the LMC. Metallicity values are binned on a 10×10 coordinate grid. In each bin, we compute the average metallicity and the associated errors which are due to the uncertainties in the determination of the Fourier parameter ϕ_{31} and are shown in each grid box.

licity and their statistical uncertainty were estimated in each spatial bin. The metallicity values considered here are those of $[Fe/H]_I$ determined in this study.

7 SUMMARY AND CONCLUSIONS

In this paper, we have undertaken a careful and systematic study of the RRab stars present in the OGLE-III catalog. The cleaned phased light curves were utilized in order to obtain various Fourier parameters. All the Fourier parameters needed for the analysis of the RRab stars are provided with their errors. Precise selection criteria were employed to get a clean sample of the RRab stars for further analysis. The application of the ‘compatibility test’ of JK96 based on the calculation of the deviation parameters yields 13,095 ‘normal-looking’ RRab stars. The light curves of these 13,095 RRab stars were analyzed further for determination of their metallicities and distances enabling us to study the structure of the LMC.

The representation of RRab stars on $P - \phi_{31}^V$ diagram clearly shows the existence of three significant metallicity groups with mean metallicities -1.20 ± 0.12 dex, -1.57 ± 0.10 dex and -1.89 ± 0.09 dex. The corresponding absolute magnitudes of these three groups are obtained as 0.70 ± 0.08 mag, 0.59 ± 0.06 mag and 0.49 ± 0.08 mag, respectively. Distribution of these three groups as a function of vertical $|z|$ distance indicates that majority of the stars belonging to each group are concentrated upto ~ 10 kpc which traces the disk of the LMC. The distribution beyond $|z| = 10$ kpc suggests the existence of an inner halo of the LMC, where most of the stars are metal poor belonging to groups II and III. Since the majority of the old and metal poor stars ($> 91\%$) are located within $|z| = 10$ kpc, it may be concluded

that the disk of the LMC has been formed much earlier than the extended halo.

The structure of the LMC has been studied using the distance distribution of the 13,095 RRab stars. The coordinates (α, δ) and the individual distances D of the RRab stars were converted into the Cartesian coordinates with the origin at the LMC center (α_0, δ_0) and the mean distance to the LMC D_0 . Approximating the LMC disk as a tri-axial ellipsoid, we have used the principal axes transformation of the moment of inertia tensor obtained from the distribution of the selected sample of RRab stars. The following geometrical parameters have been determined: inclination $i = 24^\circ.20$ and position angle of the line of nodes $\theta_{lon} = 176^\circ.01$.

The question of existence of metallicity gradient in the LMC has been studied using the $P - A_V - [Fe/H]$ empirical relation and the $P - \phi_{31} - [Fe/H]$ relations. We did not find any evidence of a radial metallicity gradient in the LMC within the uncertainties of their values. Accurate spectroscopic measurements are needed to confirm findings.

ACKNOWLEDGMENTS

HPS acknowledges Indo-US Science & Technology Forum (IUSSTF) for supporting the Indo-US Joint Center on Analysis of Variable Star Data. The authors acknowledge helpful discussions with Shashi Kanbur. SD thanks Department of Science & Technology (DST), Govt. of India for support under Fast Track Scheme for Young Scientist in Physical Sciences. The study made use of arxiv.org/archive/astro-ph and NASA ADS databases. The authors thank the anonymous referee for many useful comments and suggestions that significantly improved the paper.

REFERENCES

- Alcock C., Allsman R. A., Alves D. R., Axelrod T. S., Basu A., Becker A. C., Bennett D. P., Cook K. H., Drake A. J., Freeman K. C., Geha M., Griest K., King L., Lehner M. J., Marshall S. L., Minniti D. a., 2000, *AJ*, 119, 2194
- Arellano Ferro A., Giridhar S., Bramich D. M., 2010, *MNRAS*, 402, 226
- Bernard E. J., Gallart C., Monelli M., Aparicio A., Cassisi S., Skillman E. D., Stetson P. B., Cole A. A., Drozdovsky I., Hidalgo S. L., Mateo M., Tolstoy E., 2008, *ApJ*, 678, L21
- Bevington P., Robinson D., 2003, *Data reduction and error analysis for the physical sciences*. McGraw-Hill Higher Education, McGraw-Hill
- Butler D. J., 2003, *A&A*, 405, 981
- Cacciari C., Corwin T. M., Carney B. W., 2005, *AJ*, 129, 267
- Cáceres C., Catelan M., 2008, *ApJS*, 179, 242
- Carrera R., Gallart C., Aparicio A., Hardy E., 2011, *AJ*, 142, 61
- Catelan M., Pritzl B. J., Smith H. A., 2004, *ApJS*, 154, 633
- Challouf M., Nardetto N., Mourard D., Aroui H., Chesneau O., 2012, in Boissier S., de Laverny P., Nardetto N., Samadi R., Valls-Gabaud D., Wozniak H., eds, *SF2A-2012: Proceedings of the Annual meeting of the French Society of Astronomy and Astrophysics Calibration of the*

- surface-brightness relation of B early type stars: Towards a very accurate distance determination of LMC eclipsing binaries. pp 299–303
- Cioni M.-R. L., 2009, *A&A*, 506, 1137
- Clementini G., 2010, in Sterken C., Samus N., Szabados L., eds, *Variable Stars, the Galactic halo and Galaxy Formation RR Lyrae Stars in Dwarf Spheroidal Galaxies*. p. 107
- de Grijs R., 2011, *An Introduction to Distance Measurement in Astronomy*. Wiley
- de Vaucouleurs G., Freeman K. C., 1972, *Vistas in Astronomy*, 14, 163
- Deb S., Singh H. P., 2010, *MNRAS*, 402, 691
- Deb S., Singh H. P., 2011, *MNRAS*, 412, 1787
- Di Criscienzo M., Marconi M., Caputo F., 2004, *ApJ*, 612, 1092
- Feast M. W., Abedigamba O. P., Whitelock P. A., 2010, *MNRAS*, 408, L76
- Freedman W. L., Madore B. F., Gibson B. K., Ferrarese L., Kelson D. D., Sakai S., Mould J. R., Kennicutt Jr. R. C., Ford H. C., Graham J. A., Huchra J. P., Hughes S. M. G., Illingworth G. D., Macri L. M., Stetson P. B., 2001, *ApJ*, 553, 47
- Fukui Y., Kawamura A., 2010, *ARA&A*, 48, 547
- Glatt K., Grebel E. K., Koch A., 2010, *A&A*, 517, A50
- Grocholski A. J., Cole A. A., Sarajedini A., Geisler D., Smith V. V., 2006, *AJ*, 132, 1630
- Haschke R., Grebel E. K., Duffau S., 2012, *AJ*, 144, 106
- Haschke R., Grebel E. K., Duffau S., Jin S., 2012, *AJ*, 143, 48
- Huang L., 2011, *A Concise Introduction to Mechanics of Rigid Bodies: Multidisciplinary Engineering*. Springer-Link : Bücher, Springer
- Jurcsik J., 1995, *Acta Astronomica*, 45, 653
- Jurcsik J., 1998, *A&A*, 333, 571
- Jurcsik J., Kovacs G., 1996, *A&A*, 312, 111 [JK96]
- Karnesky R. A., Sudbrack C. K., Seidman D. N., 2007, *Scripta Materialia*, 57, 353
- Kim S., Staveley-Smith L., Dopita M. A., Freeman K. C., Sault R. J., Kesteven M. J., McConnell D., 1998, *ApJ*, 503, 674
- Kinemuchi K., Smith H. A., Woźniak P. R., McKay T. A., ROTSE Collaboration 2006, *AJ*, 132, 1202
- Klein C. R., Richards J. W., Butler N. R., Bloom J. S., 2011, *ApJ*, 738, 185
- Koerwer J. F., 2009, *AJ*, 138, 1
- Kovacs G., Jurcsik J., 1996, *ApJ*, 466, L17
- Kovacs G., Kanbur S. M., 1998, *MNRAS*, 295, 834
- Kovács G., Walker A. R., 2001, *A&A*, 371, 579
- Lin D. N. C., Jones B. F., Klemola A. R., 1995, *ApJ*, 439, 652
- Majaess D., Turner D., Gieren W., Lane D., 2012, *ApJL*, 752, L10
- Nemec J. M., Smolec R., Benko J. M., Moskalik P., Kolenberg K., Szabo R., Kurtz D. W., Bryson S., Guggenberger E., Chadid M., Jeon Y.-B., Kunder A., Layden A. C., Kinemuchi 2011, *MNRAS*, 417, 1022
- Nikolaev S., Drake A. J., Keller S. C., Cook K. H., Dalal N., Griest K., Welch D. L., Kanbur S. M., 2004, *ApJ*, 601, 260
- Pejcha O., Stanek K. Z., 2009, *ApJ*, 704, 1730
- Persson S. E., Madore B. F., Krzemiński W., Freedman W. L., Roth M., Murphy D. C., 2004, *AJ*, 128, 2239
- Piatti A. E., Geisler D., 2013, *AJ*, 145, 17
- Pietrzyński G., Graczyk D., Gieren W., Thompson I. B., Pilecki B., Udalski A., Soszyński I., Kozłowski S., Konorski P., Suchomska K., Bono G., Moroni P. G. P., Villanova S., 2013, *NATURE*, 495, 76
- Press W. H., Teukolsky S. A., Vetterling W. T., Flannery B. P., 2002, *Numerical recipes in C++ : the art of scientific computing*
- Riess A. G., Macri L., Casertano S., Lampeitl H., Ferguson H. C., Filippenko A. V., Jha S. W., Li W., Chornock R., 2011, *ApJ*, 730, 119
- Rubele S., Kerber L., Girardi L., Cioni M.-R., Marigo P., Zaggia S., Bekki K., de Grijs R., Emerson J., Groenewegen M. A. T., Gullieuszik M., Ivanov V., Miszalski B., Oliveira J. M., Tatton B., van Loon J. T., 2012, *A&A*, 537, A106
- Saha A., Hoessel J. G., 1990, *AJ*, 99, 97
- Sandage A., 2004, *AJ*, 128, 858
- Sandage A., Cacciari C., 1990, *ApJ*, 350, 645
- Schaefer B. E., 2008, *AJ*, 135, 112
- Schlegel D. J., Finkbeiner D. P., Davis M., 1998, *ApJ*, 500, 525
- Smolec R., 2005, *Acta Astronomica*, 55, 59
- Sollima A., Cacciari C., Valenti E., 2006, *MNRAS*, 372, 1675
- Soszyński I., Udalski A., Szymanski M., Kubiak M., Pietrzyński G., Wozniak P., Zebrun K., Szewczyk O., Wyrzykowski L., 2003, *Acta Astronomica*, 53, 93
- Soszyński I., Udalski A., Szymański M. K., Kubiak M., Pietrzyński G., Wyrzykowski L., Szewczyk O., Ulaczyk K., Poleski R., 2009, *Acta Astron.*, 59, 1 [SZ09]
- Subramaniam A., 2003, *ApJL*, 598, L19
- Subramaniam A., Subramanian S., 2009, *A&A*, 503, L9
- Subramanian S., Subramanian A., 2010, *A&A*, 520, A24
- Subramanian S., Subramanian A., 2012, *ApJ*, 744, 128
- Subramanian S., Subramanian A., 2013, *A&A*, 552, A144
- Tang K., 2006, *Mathematical Methods for Engineers and Scientists 1: Complex Analysis, Determinants and Matrices*. *Mathematical Methods for Engineers and Scientists*, Springer
- Udalski A., Kubiak M., Szymanski M., 1997, *Acta Astronomica*, 47, 319
- van den Bergh S., 1988, *PASP*, 100, 1486
- van der Marel R. P., Cioni M.-R. L., 2001, *AJ*, 122, 1807
- Vilardell F., Ribas I., Jordi C., Fitzpatrick E. L., Guinan E. F., 2010, *A&A*, 509, A70
- Wagner-Kaiser R., Sarajedini A., 2013, *MNRAS*, 431, 1565
- Weinberg M. D., Nikolaev S., 2001, *ApJ*, 548, 712
- Westerland B. E., 1997, *The Magellanic Clouds*
- Woźniak P. R., Vestrand W. T., Akerlof C. W., Balsano R., Bloch J., Casperson D., Fletcher S., Gisler G., Kehoe R., Kinemuchi K., Lee B. C., Marshall S., McGowan K. E., McKay T. A., Rykoff E. S., Smith D. A., Szymanski J., Wren J., 2004, *AJ*, 127, 2436
- Zinn R., West M. J., 1984, *ApJS*, 55, 45 [ZW84]